MOLECULAR AND CELLULAR BIOLOGY, Oct. 2000, p. 7706–7715 Vol. 20, No. 20
0270-7306/00/$04.00+0

No Obvious Abnormality in Mice Deficient in Receptor Protein Tyrosine Phosphatase β

S. HARROCH,[1] M. PALMERI,[1] J. ROSENBLUTH,[2] A. CUSTER,[3] M. OKIGAKI,[1] P. SHRAGER,[3] M. BLUM,[4] J. D. BUXBAUM,[5] AND J. SCHLESSINGER[1]*

Department of Pharmacology and the Skirball Institute[1] and Department of Physiology and Neuroscience,[2] New York University Medical Center, New York, New York 10016; Department of Neurobiology and Anatomy, University of Rochester Medical Center, Rochester, New York 14642[3]; and Departments of Neurobiology[4] and Psychiatry,[5] Mount Sinai School of Medicine, New York, New York 10029

Received 27 April 2000/Returned for modification 30 June 2000/Accepted 12 July 2000

The development of neurons and glia is governed by a multitude of extracellular signals that control protein tyrosine phosphorylation, a process regulated by the action of protein tyrosine kinases and protein tyrosine phosphatases (PTPs). Receptor PTPβ (RPTPβ; also known as PTPζ) is expressed predominantly in the nervous system and exhibits structural features common to cell adhesion proteins, suggesting that this phosphatase participates in cell-cell communication. It has been proposed that the three isoforms of RPTPβ play a role in regulation of neuronal migration, neurite outgrowth, and gliogenesis. To investigate the biological functions of this PTP, we have generated mice deficient in RPTPβ. RPTPβ-deficient mice are viable, are fertile, and showed no gross anatomical alterations in the nervous system or other organs. In contrast to results of in vitro experiments, our study demonstrates that RPTPβ is not essential for neurite outgrowth and node formation in mice. The ultrastructure of nerves of the central nervous system in RPTPβ-deficient mice suggests a fragility of myelin. However, conduction velocity was not altered in RPTPβ-deficient mice. The normal development of neurons and glia in RPTPβ-deficient mice demonstrates that RPTPβ function is not necessary for these processes in vivo or that loss of RPTPβ can be compensated for by other PTPs expressed in the nervous system.

Protein tyrosine phosphatases (PTPs), in concert with protein tyrosine kinases (PTKs), regulate signal transduction pathways by tyrosine phosphorylation and dephosphorylation. PTPs comprise a structurally diverse family of enzymes. One group of PTPs exhibit structural features that are also common to cell surface receptors and cell adhesion molecules (CAMs), suggesting that these receptors may play a role in cell-cell communication (4, 43). These receptor-like PTPs (RPTPs) are composed of an extracellular domain, a single transmembrane domain, and a cytoplasmic portion that contains one or two tyrosine phosphatase domains. RPTPβ (also known as PTPζ) and RPTPγ are two members of a subfamily of RPTPs that contain a region in their extracellular domains that has sequence homology to the enzyme carbonic anhydrase (CAH) (2, 3, 24, 25). In both RPTPβ and RPTPγ, the CAH domain is followed by a fibronectin domain type III repeat and by a long unique sequence termed the spacer domain. Three different isoforms of RPTPβ are expressed as a result of alternative mRNA splicing: a short and a long form that differ by the presence of a stretch of 860 amino acid residues in the spacer domain and a secreted form composed of only the extracellular domain of RPTPβ, also known as 3F8 proteoglycan or phosphacan. Both transmembrane RPTPβs and the phosphacan isoform are predominantly expressed as chondroitin sulfate proteoglycans.

Previous studies have suggested a role for RPTPβ in gliogenesis and neuron-glial cell interaction, neurite outgrowth, and neuronal migration, as well as in regeneration after injury (21, 26, 43).

RPTPβ is expressed predominantly by glial cells, astroglia, oligodendrocytes, and Schwann cells but also by neurons throughout the developing and adult nervous system (5, 41). Both transmembrane forms of RPTPβ are predominantly expressed in glial progenitors cells located in the ventricular and subventricular zone, where active cell proliferation occurs. Phosphacan is expressed at high levels by more mature glial cells, which suggests that the expression of RPTPβ is regulated during glial cell differentiation (6). Furthermore, RPTPβ expressed at the surface of glial cells binds to a cell recognition complex on neurons consisting of several proteins which include contactin, Caspr (also named paranodin) (34, 35), and Nr-CAM (40). On the basis of the localization of Caspr at the paranode, it was suggested that RPTPβ is involved in myelination and formation of the node (10).

RPTPβ has been shown to bind to a variety of CAMs and matrix components such as tenascin (18), Nr-CAM (40), L1, contactin (34), and pleiotrophin (28). Overlapping localization of phosphacan and most of the binding proteins is observed in the central nervous system (CNS), suggesting that these interactions could occur in vivo and may be involved in the control of cell proliferation, migration, adhesion, neurite outgrowth, and pathfinding in the brain. It was shown that chondroitin sulfate proteoglycans and CAM are often upregulated during brain damage or nerve injury (12, 30). Furthermore, it was demonstrated that RPTPβ is upregulated after sciatic nerve crushes, suggesting a role of RPTPβ in regeneration after injury (26).

The three isoforms of RPTPβ are expressed throughout the developing and adult nervous system. Interestingly, phosphacan binds to neurons and inhibits adhesion and neurite out-

* Corresponding author. Mailing address: Department of Pharmacology, New York University Medical Center, 550 First Ave., New York, NY 10016. Phone: (212) 263-7111. Fax: (212) 263-7133. E-mail: Schlej01@popmail.med.nyu.edu.

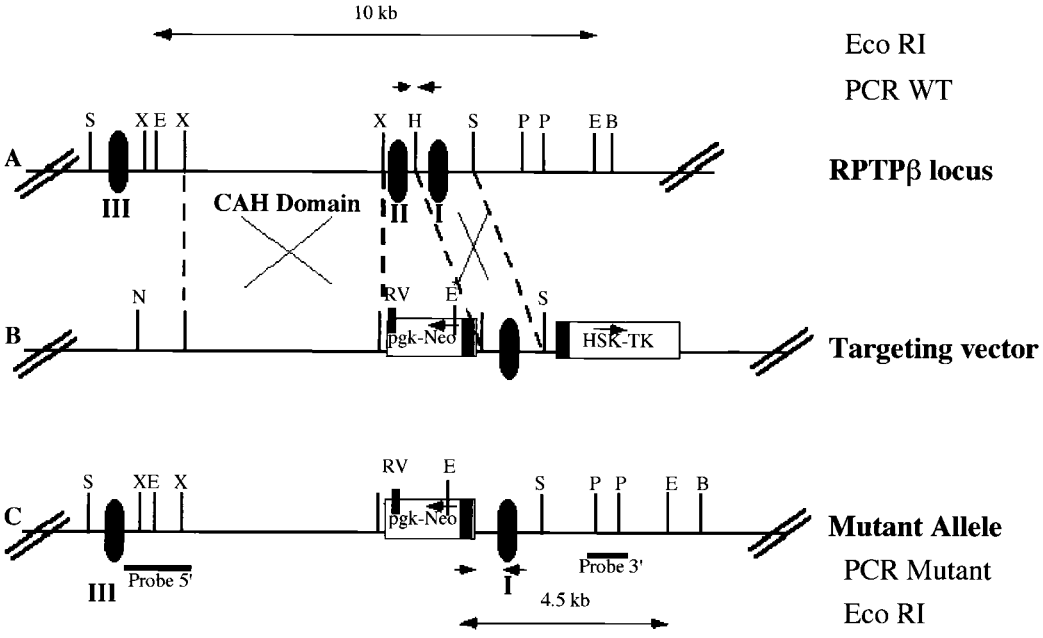

FIG. 1. RPTPβ gene organization and structure of the disrupted RPTPβ gene. (A) Restriction map of the mouse RPTPβ gene. Translated exons are represented by closed boxes and numbered I to III. E, B, H, P, RV, S, and X represent cleavage sites for *Eco*RI, *Bam*HI, *Hin*dIII, *Pst*I, *Eco*RV, *Sac*I, and *Xba*I (not all sites given), respectively. WT, wild type. (B) Restriction map of the RPTPβ-targeting construct p5′PGKneo3′TK, containing 4 and 2.1 kb of homologous sequences on the 5′ and 3′ sites of the *neo* insertion, respectively. *pgk-neo* and HSV *tk* cassettes are indicated by boxes. Arrows indicate transcriptional orientation of the genes. N represents cleavage site for *Not*I. (C) Structure of the RPTPβ gene after homologous recombination and localization of probes. Horizontal bars indicate the localization of 5′ and 3′ hybridization probes. Small arrows represent the position of the oligonucleotide used for PCR analysis.

growth (13, 17). In contrast, the extracellular portion of RPTPβ has been shown to induce neurite outgrowth. RPTPβ induces neurite outgrowth through its interaction with contactin and Nr-CAM (40). In addition, phosphacan can also stimulate neurite outgrowth of mesencephalic and hippocampal neurons (11). It was demonstrated that heterophilic interaction between RPTPβ and pleiotrophin mediates cell migration of cortical neurons, a process blocked by the PTP inhibitor sodium vanadate (28). Moreover, it has been shown that mesencephalic dopaminergic (DA) neurons express phosphacan. A heterophilic interaction between phosphacan on the neurons and L1 on the fibers may be involved in the control of migration of mesencephalic DA neurons (33), suggesting that RPTPβ may play a more general role in cell migration.

To explore the biological function of RPTPβ in vivo, we have generated mice deficient in the three isoforms of RPTPβ. These RPTPβ$^{-/-}$ mice are viable and fertile and showed no gross anatomical alterations. We have tested the importance of RPTPβ in myelination, neurite outgrowth, and node formation in the adult mouse. Our results demonstrate that RPTPβ is not required for neurite outgrowth and paranode formation, in contrast to what has been proposed based on in vitro experiments. However, ultrastructure of the CNS nerves suggests a fragility of the myelin but with no alteration of conduction velocity.

MATERIALS AND METHODS

RPTPβ targeting vector. A genomic clone containing one part of the CAH domain of the RPTPβ gene was isolated from a λFIXII mouse genomic library (129SV/Ev strain; Stratagene) by hybridization with a rat cDNA fragment corresponding to the CAH domain. A targeting vector was designed to contain 4.1 kb of 5′ homologous sequence, a *pgk-neo* cassette (42) replacing one exon in the opposite direction to RPTPβ gene transcription, 2.1 kb of 3′ homologous sequence, and the herpes simplex virus (HSV) thymidine kinase gene (*tk*). Embryonic stem (ES) cells were grown on mitomycin C-treated primary embryonic fibroblasts that had been extracted from day 15 embryos at 37°C in Dulbecco's modified Eagle's medium supplemented with 15% heat-inactivated fetal bovine serum (HyClone), 0.1 mM 2 mercaptoethanol, 1 mM sodium pyruvate, and 10^3 U of leukemia inhibitory factor (GIBCO) per ml. Cells (7×10^6) were electroporated in 800 μl of phosphate-buffered saline (PBS) with 32 μg of *Not*I-linearized targeting vector DNA at 240 V and 500 mF using a gene pulser (Bio-Rad) and plated on gelatin-coated plastic dishes. After 48 h, the cells were transferred to growth medium supplemented with G418 (150 μg/ml; GIBCO) and ganciclovir (2 μg/ml; Syntex). ES cell clones were screened by PCR using the enzyme Expand (Boehringer) and oligonucleotides located in the *neo* gene and in RPTPβ gene. Positive clones were then confirmed by Southern blot analysis. To accomplish this, genomic DNA was digested with *Eco*RI, transferred onto nylon filters, and hybridized with a radioactively labeled *Pst*I fragment from the original phage clone (Fig. 1). Three independent targeted ES clones were used in embryo aggregation experiments for generation of mice. Chimeric mice were crossed to Swiss Webster mice. Heterozygous and homozygous animals were identified by PCR and Southern blot analysis.

RNA preparation and Northern blot analysis. Total RNAs from brains of RPTPβ$^{+/+}$, RPTPβ$^{+/-}$, and RPTPβ$^{-/-}$ mice were isolated by the guanidine thiocyanate method (7). RNA were electrophoresed in a 1% agarose gel containing 7% formaldehyde and transferred to a nylon membrane (Schleicher & Schuell). Hybridization was performed with a radiolabeled 500-bp mouse cDNA probe coding for the CAH domain in 0.25 M sodium phosphate buffer (pH 7.4)–7% sodium dodecyl sulfate, followed by autoradiography.

Primary antibodies. Rabbit polyclonal antibody against CasprI was a gift from E. Peles and used at a dilution of 1:5,000; rabbit polyclonal antibody against ankyrin$_G$, a gift from S. Lux, was used at a dilution of 1:500. Mouse monoclonal antibody against the sodium channel (previously characterized by Rasband et al. [37]) was used at a dilution of 1:10,000. Rabbit anti-rat tyrosine hydroxylase (TH) polyclonal antibody (Pel-Freeze) was used at 1:1,000.

TH staining. Mice were anesthetized and transcardially perfused with ice-cold saline followed by perfusion with 4% paraformaldehyde (PFA) in 0.1 M phosphate buffer, pH 7.4 (PB). The brains were removed, cut into 3- to 4-mm blocks containing the midbrain, and postfixed in 4% PFA for 5 h. Subsequently, the brain blocks were placed in cold 30% sucrose in 0.1 M PB overnight, and 40-μm vibratome sections were cut. Using a random start, a 1:8 series of sections was collected for TH immunocytochemistry. Free-floating sections were incubated overnight at 4°C with a rabbit anti rat-TH polyclonal antibody (Pel-Freeze) (1:1,000 in PBS–3% goat serum–0.3% Triton X-100). After removal of the primary antibody and a wash with PBS, the sections were incubated for 2 h at room temperature with anti-rabbit immunoglobulin G conjugated with biotin (Amersham) (1:200 in PBS–3% goat serum–0.3% Triton X-100). The secondary

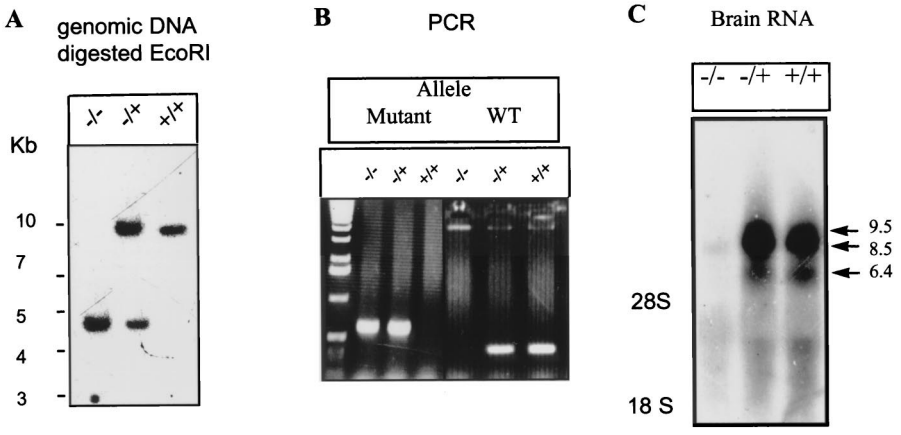

FIG. 2. Southern, PCR, Northern, and immunoblot analyses of wild-type and RPTPβ-deficient mice. (A) Southern blot analysis. DNA from wild-type, RPTPβ$^{-/+}$, and RPTPβ$^{-/-}$ mice digested with *Eco*RI was hybridized with a 3′ probe (*Pst*I probe). The 10-kb band represents the wild-type allele, and the 4.5-kb band represents the mutant allele. (B) PCR analyses. For easy screening, we used a PCR wherein the wild-type (WT) allele is amplified as a 500-bp DNA and the mutant allele is amplified as a 300-bp product. (C) Northern blot analysis. RNA from brains of RPTPβ$^{+/+}$, RPTPβ$^{-/-}$, and RPTPβ$^{-/+}$ mice was hybridized with a 500-bp cDNA fragment encoding the mouse CAH domain. Arrows point to the three transcripts of RPTPβ in both wild-type and heterozygous RNAs that are absent in RPTPβ$^{-/-}$ mice. Sizes are indicated in kilobases.

antibody was removed, sections were washed, the reaction was quenched for 5 min in 0.3% H_2O_2 in PBS, and the samples were incubated with ExtraAvidin-peroxidase (1:200; Sigma) for 1 h before being incubated with 3,3′-diaminobenzidine.

Light microscopy. Mice were deeply anesthetized and perfused through the left ventricle with 3% PFA in 0.1 M PB. Brains were removed and postfixed in the same fixative overnight, washed in PB, and embedded in paraffin. Sections of 6 μm were cut and stained with cresyl violet. For Timm staining, mice were perfused through the left ventricle with sodium sulfide solution (19) followed by 4% PFA. Then 6-μm paraffin sections were mounted and stained in darkness at 24°C as described elsewhere (19). After staining for 15 or 45 min, the sections were counterstained with cresyl, dehydrated, and coverslipped.

Electron microscopy. Mice were anesthetized with pentobarbital and perfused transcardially with a fixative consisting of 3% glutaraldehyde and 2% PFA in 0.1 M cacodylate buffer (pH 7.3). Optic nerve and spinal cord segments were dissected out, rinsed, postfixed in 1 to 2% osmium tetroxide, with or without added 1.5% potassium ferricyanide, in 0.1 M cacodylate buffer, dehydrated in a graded series of alcohols, and embedded in Araldite or an Epon-Araldite mixture. Sections of 1 μm were cut with glass knives and stained with 1% toluidine blue for survey by light microscopy. Selected areas were then sectioned at ~0.1 μm, mounted on copper grids, stained with potassium permanganate followed by ethanolic uranyl acetate, and examined in a Philips 300 electron microscope. Both cross and longitudinal sections were studied. Animals studied ranged in age from 2 to 9.5 months.

Suction electrode recording. Mouse optic nerves were dissected and placed in a recording chamber that was continuously perfused and temperature regulated. The standard Locke's solution contained NaCl (154 mM), KCl (5.6 mM), $CaCl_2$ (2 mM), D-glucose (5.6 mM), and HEPES (10 mM, pH 7.4). For stimulation and recording of compound action potentials (CAPs), each end of the nerve was drawn into a suction electrode. Stimuli consisted of 50-μs pulses that were adjusted to 10% above the level required for a maximal response. After a stimulus, CAPs were amplified, digitized, recorded, and analyzed with a laboratory computer. Conduction velocity was calculated as the length of the nerve divided by the time to the first peak amplitude of the CAP. For some experiments, CAPs were measured, and then nerves were fixed and used for labeling experiments.

Immunocytochemistry. Optic nerves were dissected, fixed in 4% PFA (pH 7.2) for 30 min, and soaked overnight in 20% sucrose at 4°C. The nerves were then frozen in OCT mounting medium (Miller), cut into 10-μm sections on a microtome, and dried on gelatin-coated coverslips. The sections were incubated in PBTGS (45 ml of 0.1 M PB, 150 μl of Triton X-100, 5 ml of goat serum) for 1 to 2 h to permeabilize and block. All subsequent solutions used PBTGS for dilutions or washing, and all incubations were done at room temperature. Three washes of 5 min were done after each antibody incubation. Rabbit polyclonal antibodies were applied first for 15 h. Anti-rabbit Alexa 488 (1:500; Molecular Probes, Eugene, Oreg.) was then added for 1 h. For double labeling, mouse monoclonal antibodies were added for 15 h, and anti-mouse Cy3 (1:500; Accurate Chemicals, Westbury, N.Y.) was applied for 1 h. Sections were then washed serially in PBTGS, 0.1 M PB, and 0.05 M PB and allowed to air dry. The labeled sections were mounted on slides and viewed under a Nikon Microphot-SA fluorescence microscope. Images were taken by a C4742-95 cooled charge-coupled device camera (Hamamatsu) controlled by Image Pro software (Media Cybernetics).

RESULTS

Generation of RPTPβ-deficient mice. Using a rat cDNA fragment corresponding to the CAH domain of the RPTPβ gene, a clone including a 3′ part of this domain was isolated from a mouse 129Sv/Ev genomic library. The targeting vector for the RPTPβ gene comprised 4.1 kb of 5′ homologous sequence, a *pgk-neo* cassette in opposite direction to RPTPβ gene transcription (42) replacing one exon, 2.1 kb of 3′ homologous sequence, and HSV *tk* for selection against random integration (29). Homologous recombination with this targeting vector results in a loss of exon 2 and in inadequate splicing, resulting in a null mutation.

After electroporation of the linearized targeting vector into either R1 or W4 ES cells followed by double selection with G418 and ganciclovir, approximately 1 clone out of 100 or 1 clone out of 50, respectively, carried the desired mutation as determined by PCR (data not shown) and verified by Southern blot analysis with the 3′ external probe. The presence of a new *Eco*RI site introduced by insertion of *neo* sequence into RPTPβ gene was detected by the appearance of a 4.5-kb band in addition to the wild-type band of 10 kb.

Chimeric mice were obtained after aggregation of targeted ES cells. Chimeric males showed germ line transmission of the disrupted RPTPβ gene as analyzed by Southern blot analysis. Crossing of heterozygous RPTPβ$^{-/+}$ offspring yielded homozygous RPTPβ-deficient mice with strictly Mendelian frequencies. Southern blot analysis of these mice with 3′ and 5′ external probes (Fig. 2A), as well as with a *neo* probe, showed the pattern expected for a single integration by homologous recombination (data not shown). We subsequently used PCR with a reverse oligonucleotide in the *neo* promoter and a forward oligonucleotide on the 3′ arm or in exon II to screen for homozygous animals (Fig. 1 and 2B).

To determine whether the mutated RPTPβ gene is transcribed, total RNAs from brains of RPTPβ$^{-/-}$, RPTPβ$^{-/+}$, RPTPβ$^{+/+}$ mice were subjected to Northern blot analysis. After hybridization with a mouse cDNA specific probe for the

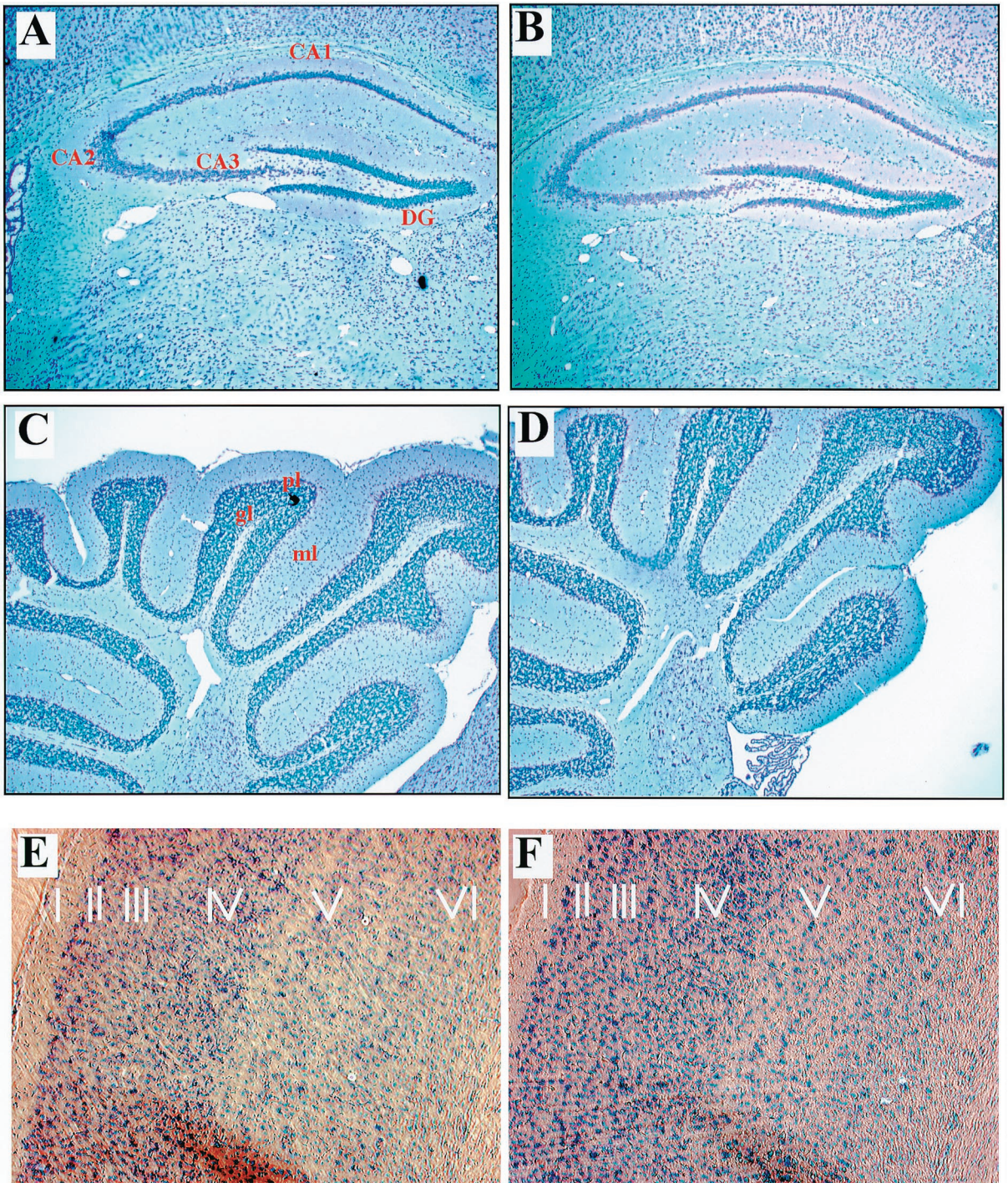

FIG. 3. Analysis of the hippocampi, cortices, and cerebella of RPTPβ-deficient mice by light microscopy. Sections of 6 μm through hippocampi (A and B), cerebella (C and D), and cortices (E and F) of adult wild-type (A, C, and E) and RPTPβ-deficient (B, D, and F) mice were stained with Nissl stain. The overall histology, number, and localization of each cell type in these regions of the brain appear normal in RPTPβ-deficient mice. ml, molecular layer; pl, Purkinge cell layer; gl, internal granular layer; DG, dentate gyrus.

CAH domain, no hybridization was detectable with RNA from RPTPβ-deficient mice, while RPTPβ mRNAs of 9.5, 8.5, and 6.4 kb were clearly detected in RPTPβ$^{-/+}$ and RPTPβ$^{+/+}$ mice, indicating that the mutated gene is not transcribed. All forms of mRNA having been lost, we therefore concluded that insertion of the mutation into the RPTPβ gene generated mice lacking the soluble form phosphacan as well as the two transmembrane forms. RPTPβ$^{-/+}$ animals showed similar amounts of RPTPβ mRNAs and were therefore used as controls.

Morphological analysis of the CNS of RPTPβ-deficient mice. At the light microscopic level, the general morphology of brains of 2-month-old RPTPβ$^{-/-}$ mice appeared normal and

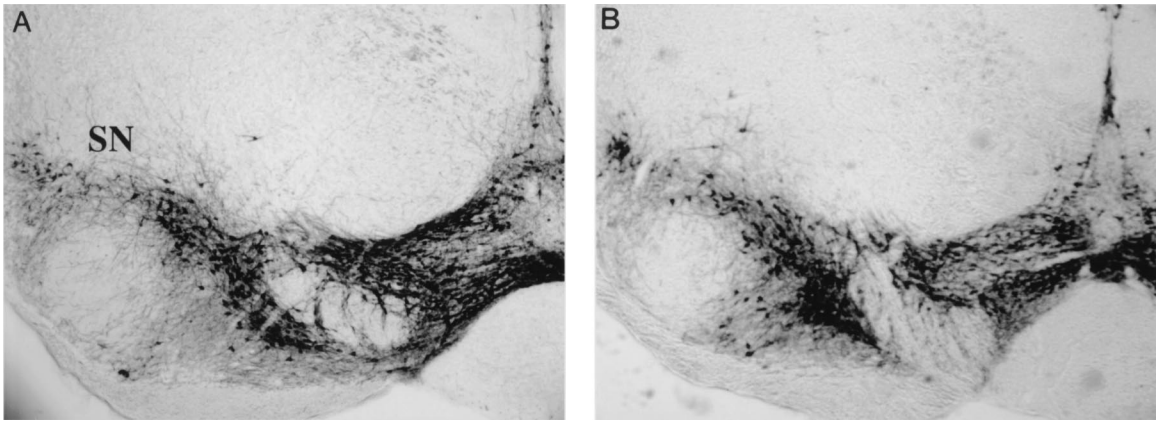

FIG. 4. Localization of mesencephalic DA neurons. Coronal sections of RPTPβ$^{-/-}$ and RPTPβ$^{-/+}$ adult animals were stained with anti-TH antibodies, revealing mesencephalic DA neurons. Wild-type and RPTPβ$^{-/-}$ DA neurons migrated properly laterally and did not localize ventrally. SN, substantia nigra.

indistinguishable from that of wild-type littermates. Cross sections through the hippocampi of RPTPβ-deficient mice displayed a normal pattern of migration of pyramidal cells in the dentate gyrus (Fig. 3A and B). In addition, we found no abnormalities in the subventricular zones of RPTPβ$^{-/-}$ mice (data not shown). In the cerebella of 2-month-old RPTPβ-deficient mice, the molecular layer, Purkinje cell layer, and internal granular cell layer appeared normal (Fig. 3C and D). Because RPTPβ is also expressed in cortical neurons (41), we also compared the lamination and organization of the cortex. We chose to look at the somatosensory cortex, where the layers are most distinguishable. The number of cells and organization in the six layers were apparently similar in wild-type and RPTPβ-deficient mice (Fig. 3E and F), indicating that RPTPβ is not necessary for cortical neuron migration. To further investigate the cortex, we examined the distribution of specific neuronal markers. Phosphacan is expressed by interneurons in the cortex (20). The calcium-binding protein parvalbumin and calbindin are expressed in distinct subpopulations of neurons. We investigated the density of inhibitory interneurons by immunocytochemistry using antibodies to the Ca^{2+}-binding protein parvalbumin as a marker for a subpopulation of GABAergic (gamma amino butyric acid) neurons. The density of parvalbumin-immunoreactive cells did not differ between wild-type and mutant animals in this region (data not shown). Immunostaining with anticalbindin (data not shown) revealed no difference in number, localization, or expression pattern between RPTPβ$^{-/-}$ and control cortex samples.

Various experiments in vitro have suggested a role of RPTPβ in neurite outgrowth. For example, RPTPβ promotes neurite outgrowth from mesencephalic and hippocampal neurons (8, 11). To test this hypothesis, we inspected the dentate gyrus of the hippocampus, where RPTPβ is highly expressed, in relation to axonal projections, the mossy fibers (MFs). MFs are the axon of the neuron, which form the granule cell layer of the dentate gyrus. MF axons of the dentate granule cells establish synaptic contacts with neurons in the dentate hilus and with pyramidal cells of the hippocampal CA3 (1). We used Timm's staining, which specifically reveals MFs and their synaptic expansion, to study MFs in RPTPβ$^{-/-}$ and control mice. Timm's stain of wild-type and RPTPβ$^{-/-}$ hippocampus sections did not reveal reduced staining or an alteration of the distribution of the fibers in RPTPβ$^{-/-}$ mice (data not shown).

Normal migration of mesencephalic neurons in RPTPβ$^{-/-}$ mice. Mesencephalic DA neurons, generated in the ventricular zone of the mesencephalon, migrate first ventrally from the ventricular surface along radial glial processes and then laterally along tangentially arranged nerve fibers to their destinations, the substantia nigra pars compacta, the reticular formation, and the ventral tegmental area. The expression of phosphacan by DA neurons and its interaction with L1 and Ng-CAM have implicated a role for it in the lateral migration of DA neurons (33). This study showed that the laterally migrating substantia nigra DA neurons express phosphacan. Since the ventral tegmental DA neurons seem to migrate only radially, they may not require phosphacan for proper migration. Thus, in the absence of phosphacan, we may observe all DA neurons clustered in the ventral tegmental area, with an absence of DA neurons in the substantia nigra. Migration of DA neurons was histologically examined in RPTPβ-deficient mice and control animals by a series of sections through the midbrain stained with an antibody directed against TH, a DA-synthesizing enzyme. As seen in Fig. 4, DA neurons migrate properly in RPTPβ-deficient mice.

Electron microscopy of optic nerves of RPTPβ-deficient mice. RPTPβ is expressed by cells of the oligodendrocyte lineage during development and in the adult (6). It has been suggested that RPTPβ is involved in formation of the node of Ranvier (10). We evaluated myelination in 2-month-old brains stained with luxol fast blue, a stain specific for myelin, and detected no difference in staining between wild-type and RPTPβ$^{-/-}$ mice (data not shown).

We then analyzed the ultrastructure of myelin in the optic nerves of animals at various ages. Myelin in the optic nerves and spinal cords of both old and adult RPTPβ$^{-/-}$ mice is grossly normal in appearance (Fig. 5A and B) with respect to periodicity and thickness. As in the wild-type animals, myelin thickness in the RPTPβ$^{-/-}$ animals increases with fiber diameter. The radial component is present, and the inner and outer mesaxons form tight junctions (Fig. 5D). In comparison with wild-type controls, however, there is a greater tendency for fragmentation of the RPTPβ$^{-/-}$ myelin (i.e., separation and disintegration of lamellae), especially in thicker sheaths (Fig. 5C), and for deformation of the myelin sheath profiles, resulting in redundant folds (Fig. 5C) (38). In addition, in the myelin sheaths of RPTPβ$^{-/-}$ animals, cytoplasm-containing lamellae can be found extending into juxtaparanodal regions (Fig. 6D) as well as in internodal myelin (Fig. 5C).

Nodal and paranodal areas in the RPTPβ$^{-/-}$ animals also appear grossly normal. The nodal gap approximates 1 μm, and

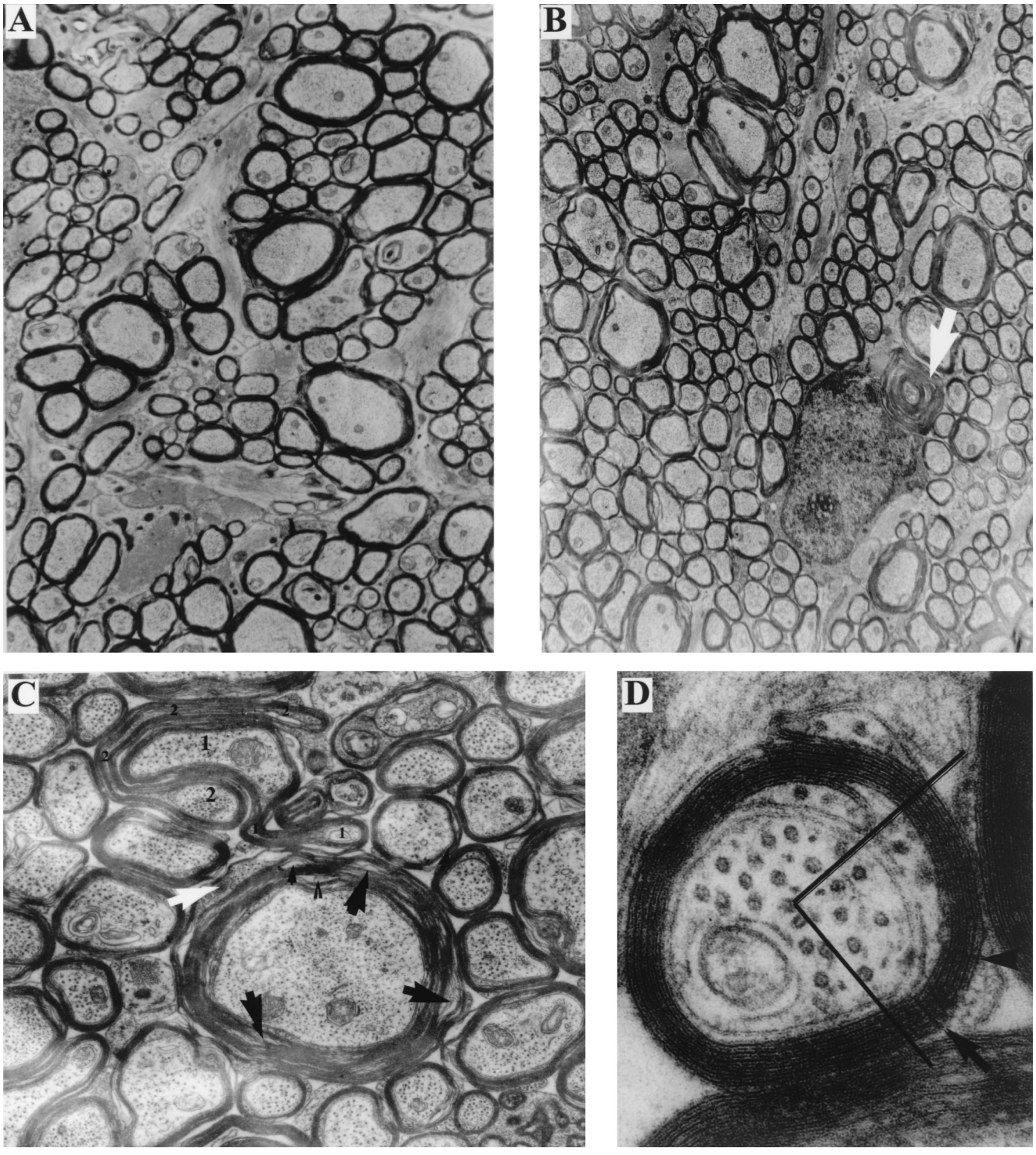

FIG. 5. Ultrastructure of the optic nerve. (A) Survey view of wild-type optic nerve cross section (magnification, ×12,600). The myelin sheaths surrounding the larger axons appears more compact than those in panel B. (B) Survey view of RPTPβ$^{-/-}$ optic nerve cross section (×12,600). In the larger fibers, myelin lamellae tend to separate. Extraneous whorls (arrow) of myelin are apposed to an oligodendrocyte. (C) Large fiber from RPTPβ$^{-/-}$ optic nerve (×31,500). The sheath appears somewhat raveled (black arrows) and in one region the lamellae contain cytoplasm (white arrow). Just above, two (large 1 and 2) fibers are surrounded by sheaths that form redundant folds (small numbers). (D) Small fiber from RPTPβ$^{-/-}$ optic nerve (×182,000). Both inner and outer mesaxons form tight junctions. Radial component (arrows) is visible in one quadrant of the sheath.

the nodal axolemma displays a typical undercoating (Fig. 6B). Paranodal loops form junctions with the axolemma. The junctional cleft is ~2 nm wide and contains transverse bands, the periodic dense ridges that extend between the membranes of the paranodal axolemma and the glial loops (Fig. 6C). In small fibers, the overlapping pattern of the terminal loops displays the normal arrangement, i.e., with the outermost loops closest to the node and ending against the axolemma (Fig. 6B). In

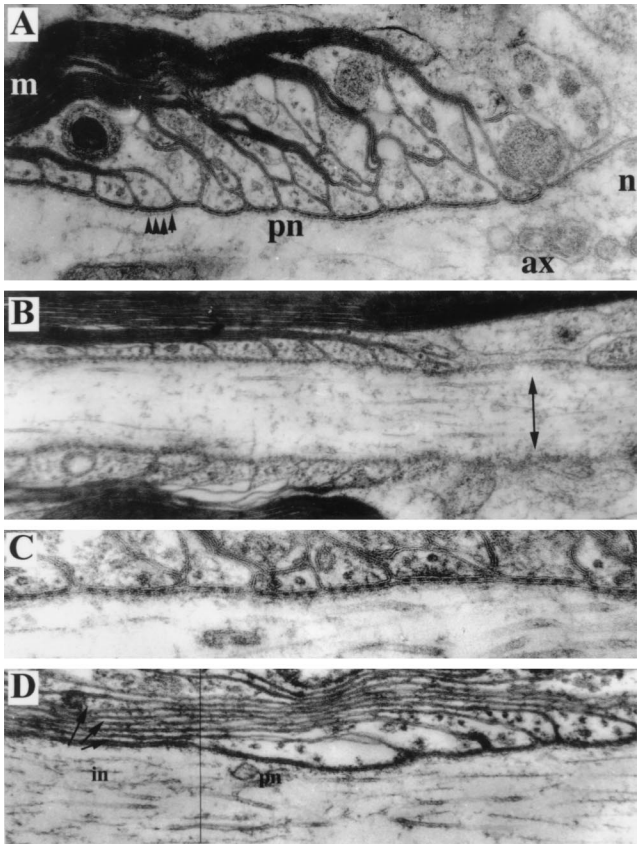

FIG. 6. Analysis of the node and paranode by electron microscopy. (A) Paranodal junction from a wild-type spinal cord (magnification, ×100,000). Some terminal loops adjoin the axolemma and form junctions containing transverse bands (arrowheads); others do not reach the axolemma. The node of Ranvier (n) is at the right. The axon (ax), paranode (pn), and myelin sheath (m) are indicated. (B) Small fiber from RPTPβ$^{-/-}$ optic nerve (×79,000). The node of Ranvier (right) shows undercoated plasma membrane (arrow). Myelin lamellae form a regular succession of overlapping terminal loops. (C) Detail of paranodal junction from a large fiber in RPTPβ$^{-/-}$ spinal cord (×152,000). Some terminal loops end against the axolemma, forming junctions containing periodic transverse bands. Not all terminal loops reach the axolemma, however. (D) Paranodal (pn) and juxtaparanodal (in) regions of axon in a large fiber from RPTPβ$^{-/-}$ spinal cord (×87,500). Cytoplasm-containing lamellae extend beyond the paranode toward the internode (arrows).

more heavily myelinated fibers of both wild-type (Fig. 6A) and RPTPβ$^{-/-}$ (Fig. 6C) animals, some of the terminal loops end either on other loops or in an everted pattern facing away from the axolemma.

Na^{2+} channel clustering, Caspr localization, and conduction velocity of the optic nerve. Recent studies suggested that RPTPβ might mediate interactions between axons and glial cells (35) through interaction with the contactin-Caspr complex. Caspr is a membrane protein highly expressed in the CNS that copurified with contactin when the CAH of RPTPβ was used as an affinity probe. It was shown that Caspr is an essential component of the paranode (10). Thus, RPTPβ could play a role in formation of the paranode and node of Ranvier. We therefore analyzed optic nerve sections, labeled for voltage-gated sodium channels to mark nodes of Ranvier and labeled for CasprI to mark paranodes (Fig. 7A). Both the nodes of Ranvier and paranodes in RPTPβ$^{-/-}$ mice exhibited normal morphology and showed similar fluorescence staining with antibody markers compared with control animals (Fig. 7A). Optic nerve sections were also labeled for ankyrin$_G$, a protein that links sodium channels to the cytoskeleton and is also located in the nodes of Ranvier (23). No differences in morphology or fluorescence intensity were seen with this label either. No difference was apparent in the number of labeled sites between RPTPβ$^{-/-}$ and control animals with any of the antibodies used (Fig. 7A).

Despite the normal clustering of Na^{2+} channels and Caspr localization in the optic nerves of RPTPβ-deficient mice, functional changes could result from the alteration in myelin structure that have been detected in the optic nerves of RPTPβ-deficient mice. To investigate the electrophysiological properties of CNS axons in RPTPβ-deficient mice, the CAPs of RPTPβ$^{-/-}$ optic nerves was recorded using suction electrodes, and conduction velocity was calculated using the fastest component of the CAP. Measurement of the conduction velocity at 25°C revealed no significant difference between RPTPβ$^{-/-}$ and normal nerves (Fig. 7B). While the conduction velocity of RPTPβ$^{-/-}$ nerves appeared to be somewhat slower than for controls at 37°C, this difference is not statistically significant ($P = 0.377$). The shape of CAPs in RPTPβ$^{-/-}$ nerves was similar to that seen in control nerves.

DISCUSSION

The mutation introduced in the RPTPβ gene abolishes expression of the three isoforms of RPTPβ, the two transmembrane isoforms and the soluble isoform (phosphacan), since we have abolished transcription of the RPTPβ gene. Nevertheless, the RPTPβ-deficient mice described in this study are normal in their gross general behavior and with respect to fertility, body weight, and life span.

The gross anatomy of the brain and spinal cord and the morphology of the cerebellum of RPTPβ-deficient mice do not show any alteration at the light microscopy level compared to their littermate controls. We could not detect aberrant localization of cells that normally express RPTPβ in the cerebellum, hippocampus, or cerebral cortex. Therefore, RPTPβ appears not to be necessary for the migration of these neural cell types to their correct locations in these areas of the CNS.

RPTPβ and RPTPγ belong to the same subfamily of RPTPs. Surprised by the lack of obvious phenotype in RPTPβ-deficient mice, we tested whether the expression of RPTPγ is altered in RPTPβ-deficient mice to compensate for RPTPβ deficiency. The expression of RPTPβ is restricted to the nervous system, while RPTPγ is ubiquitously expressed. However, certain neurons, especially cortical and hippocampal neurons, express both RPTPβ and RPTPγ. Northern blot analysis of mRNA prepared from adult RPTPβ$^{-/-}$, RPTPβ$^{-/+}$, or RPTPβ$^{+/+}$ brain mRNA showed no alteration of transcription of the RPTPγ gene, indicating that RPTPγ is not altered in RPTPβ$^{-/-}$ mice (data not shown). However, we cannot rule out the possibility that RPTPβ function in RPTPβ$^{-/-}$ mice is compensated for by another tyrosine phosphatase.

Evidence from in vitro studies suggests that RPTPβ family members play a key role in neuronal migration, neurite outgrowth, and cell adhesion. The secreted form of RPTPβ, phosphacan, is a chondroitin sulfate, highly expressed in the brain. Phosphacan inhibits nerve growth factor-induced neurite outgrowth of PC12D in culture (22) and neurite outgrowth of dorsal root ganglia explants (14). In contrast, phosphacan promotes neurite outgrowth from mesencephalic and hippocampal neurons (8). We tested whether dorsal root ganglia prepared from day 15 embryo RPTPβ$^{-/-}$ or control samples and cultured for 2 weeks showed any changes in neurite length, but we did not detect any obvious difference (data not shown). We

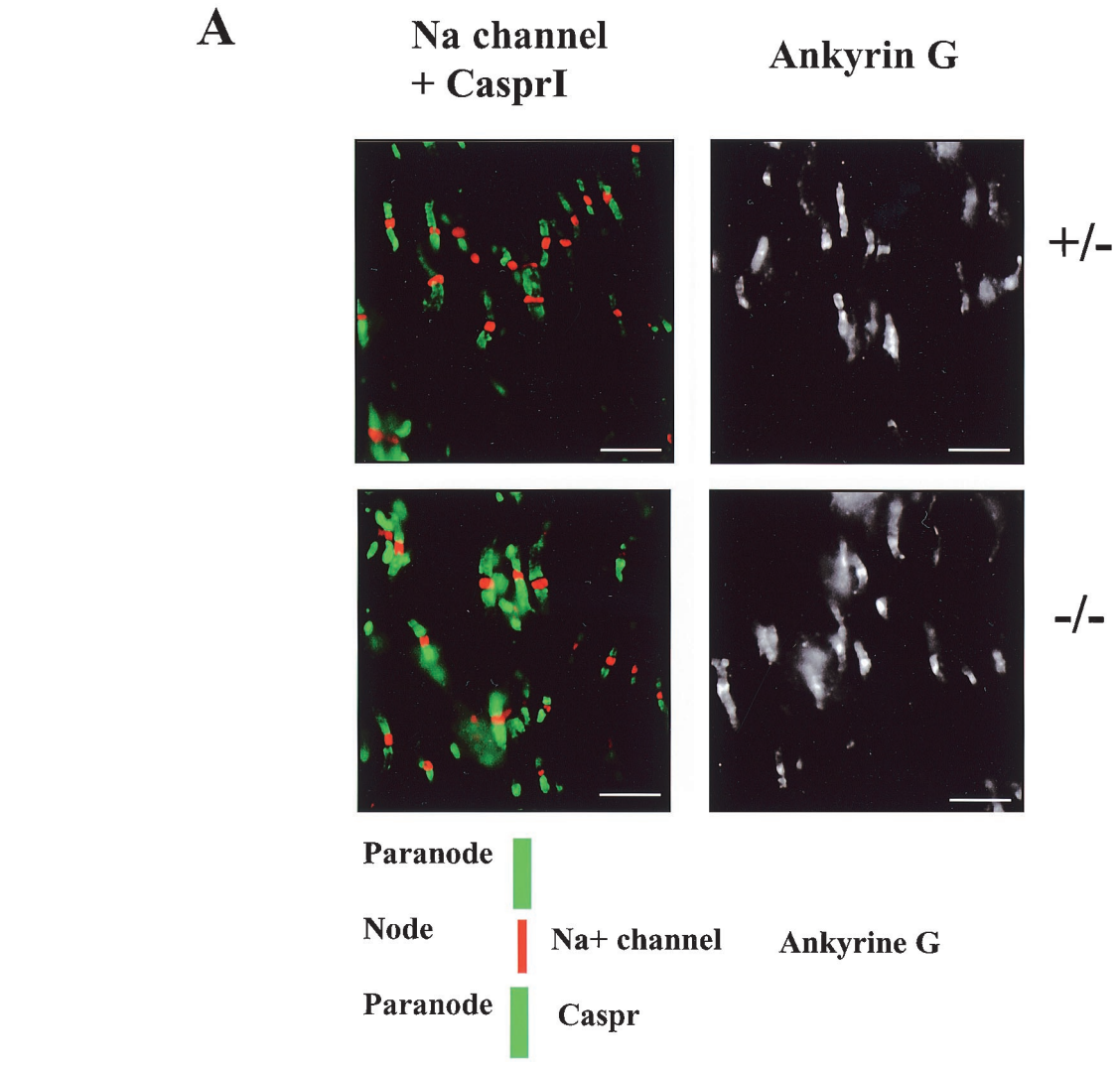

FIG. 7. Localization of Na^{2+} channels and Caspr in the optic nerve and conduction velocity measurements. Normal nodes and paranodes are found in optic nerves of RPTPβ$^{-/-}$ mice. (A) Optic nerve sections were labeled with antibodies specific for sodium channels (red), Caspr (green), and ankyrin$_G$. No apparent differences in labeling were seen between nerves from wild-type and RPTPβ$^{-/-}$ mice (scale bars = 10 μm). (B) Conduction velocity measurements of nerves from wild-type and RPTPβ$^{-/-}$ mice at 25°C (P = 0.85) or 37°C (P = 0.38). Results represent mean ± standard deviation of four nerves.

have also shown that the cells of the dentate gyrus, where RPTPβ is highly expressed, are able to produce normal MFs, as revealed by Timm and calbindin staining. Finally, we found no obvious difference in neurite length in mesencephalic neurons demonstrating, that in vivo, RPTPβ is not necessary for neurite growth.

RPTPβ isoforms are found in the developing nervous system, in patterns suggesting the involvement of these enzymes in neuronal migration and axonal guidance. RPTPβ was implicated in the differentiation of cortical neurons (27), the migration of olfactory neurons (32), and the migration of mesencephalic DA neurons (33). In the cortex, RPTPβ is expressed in layers II, III, and IV (41), and phosphacan has been found also in layers II, IV, and VI (20). Nissl stain- as well as calbindin- or parvalbumin-immunoreactive cells exhibited no difference with respect to number and localization in RPTPβ-deficient mice compared to control mice. We have also demonstrated that mesencephalic DA neurons migrate to their final destination in RPTPβ-deficient mice, suggesting that

RPTPβ does not play a major role in neuronal migration. Of course, RPTPβ could regulate the migration of a particular subset of neurons that were not detected. However, phosphacan is expressed in most parvalbumin-positive cells (20), neurons that were well localized in RPTPβ-deficient mice.

RPTPβ and myelination. Previous studies suggest that RPTPβ could be involved in the formation of the paranode. RPTPβ, contactin, and Caspr/paranodin form a complex (35) and localize to the paranodal axolemma in myelinated fibers of the peripheral nervous system and CNS (10, 31). It has been suggested that RPTPβ is expressed in oligodendrocyte paranodal loops and can interact with the Caspr-contactin complex at the surface of the axon. RPTPβ may therefore participate in formation of the paranode. However, we did not detect ultrastructural abnormalities in the paranodes of RPTPβ$^{-/-}$ animals.

RPTPβ is largely expressed in glial cells. There is also growing evidence that RPTPs may play a major role in glial differentiation because most RPTPs are expressed in oligodendrocytes and regulated during the process of maturation of oligodendrocytes (36). Expression of RPTPβ is regulated during gliogenesis (6). We could not detect any differences by light microscopy. However, analysis by electron microscopy revealed that RPTPβ$^{-/-}$ sheaths are normal in appearance but display abnormalities in the thicker sheaths, suggesting a greater susceptibility to deformation and disintegration as well as more cytoplasm-containing lamellae in regions that are normally compact. The results suggest that the RPTPβ$^{-/-}$ myelin may be less stable than normal myelin.

Abnormalities of this kind have been seen in mutants deficient in myelin glycolipids (9), myelin basic protein (15), or proteolipid protein (16, 39). The findings for RPTPβ$^{-/-}$ mice thus could reflect abnormalities in the proportions of myelin constituents. In addition, we cannot rule out the possibility that the RPTPβ$^{-/-}$ oligodendrocytes are defective and that the myelin abnormalities seen are secondary to the oligodendrocyte defects.

The results presented here provide evidence regarding the role of RPTPβ in the adult mouse. The fact that the loss of the three isoforms of RPTPβ does not grossly affect any of the processes tested raises questions about several proposed roles of RPTPβ in neurite outgrowth, cell migration, axon guidance, and gliogenesis. Our data suggest that RPTPβ is not necessary for any of these events and/or that the loss of RPTPβ may be compensated for by other PTPs expressed in the nervous system.

ACKNOWLEDGMENTS

We thank the personnel, in particular Anna Auerbach, of the NYU Medical Center Transgenic/ES Cell Chimera facility.

REFERENCES

1. **Amaral, D. G., and P. W. Menno.** 1995. Hippocampal formation, p. 443–493. *In* G. Paxinos (ed.), The rat nervous system. Academic Press, San Diego, Calif.
2. **Barnea, G., M. Grumet, P. Milev, O. Silvennoinen, J. B. Levy, J. Sap, and J. Schlessinger.** 1994. Receptor tyrosine phosphatase beta is expressed in the form of proteoglycan and binds to the extracellular matrix protein tenascin. J. Biol. Chem. **269:**14349–14352.
3. **Barnea, G., O. Silvennoinen, B. Shaanan, A. M. Honegger, P. D. Canoll, P. D'Eustachio, B. Morse, J. B. Levy, S. Laforgia, K. Huebner, et al.** 1993. Identification of a carbonic anhydrase-like domain in the extracellular region of RPTP gamma defines a new subfamily of receptor tyrosine phosphatases. Mol. Cell. Biol. **13:**1497–1506.
4. **Brady-Kalnay, S. M., and N. K. Tonks.** 1995. Protein tyrosine phosphatases as adhesion receptors. Curr. Opin. Cell Biol. **7:**650–657.
5. **Canoll, P. D., G. Barnea, J. B. Levy, J. Sap, M. Ehrlich, O. Silvennoinen, J. Schlessinger, and J. M. Musacchio.** 1993. The expression of a novel receptor-type tyrosine phosphatase suggests a role in morphogenesis and plasticity of the nervous system. Brain Res. Dev. Brain Res. **75:**293–298.
6. **Canoll, P. D., S. Petanceska, J. Schlessinger, and J. M. Musacchio.** 1996. Three forms of RPTP-beta are differentially expressed during gliogenesis in the developing rat brain and during glial cell differentiation in culture. J. Neurosci. Res. **44:**199–215.
7. **Chomczynski, P., and N. Sacchi.** 1987. Single-step method of RNA isolation by acid guanidinium thiocyanate-phenol-chloroform extraction. Anal. Biochem. **162:**156–159.
8. **Clement, A. M., S. Nadanaka, K. Masayama, C. Mandl, K. Sugahara, and A. Faissner.** 1998. The DSD-1 carbohydrate epitope depends on sulfation, correlates with chondroitin sulfate D motifs, and is sufficient to promote neurite outgrowth. J. Biol. Chem. **273:**28444–28453.
9. **Coetzee, T., N. Fujita, J. Dupree, R. Shi, A. Blight, K. Suzuki, K. Suzuki, and B. Popko.** 1996. Myelination in the absence of galactocerebroside and sulfatide: normal structure with abnormal function and regional instability. Cell **86:**209–219.
10. **Einheber, S., G. Zanazzi, W. Ching, S. Scherer, T. A. Milner, E. Peles, and J. L. Salzer.** 1997. The axonal membrane protein Caspr, a homologue of neurexin IV, is a component of the septate-like paranodal junctions that assemble during myelination. J. Cell Biol. **139:**1495–1506.
11. **Faissner, A., A. Clement, A. Lochter, A. Streit, C. Mandl, and M. Schachner.** 1994. Isolation of a neural chondroitin sulfate proteoglycan with neurite outgrowth promoting properties. J. Cell Biol. **126:**783–799.
12. **Fawcett, J. W., and R. A. Asher.** 1999. The glial scar and central nervous system repair. Brain Res. Bull. **49:**377–391.
13. **Friedlander, D. R., P. Milev, L. Karthikeyan, R. K. Margolis, R. U. Margolis, and M. Grumet.** 1994. The neuronal chondroitin sulfate proteoglycan neurocan binds to the neural cell adhesion molecules Ng-CAM/L1/NILE and N-CAM, and inhibits neuronal adhesion and neurite outgrowth. J. Cell Biol. **125:**669–680.
14. **Garwood, J., O. Schnadelbach, A. Clement, K. Schutte, A. Bach, and A. Faissner.** 1999. DSD-1-proteoglycan is the mouse homolog of phosphacan and displays opposing effects on neurite outgrowth dependent on neuronal lineage. J. Neurosci. **19:**3888–3899.
15. **Gould, R. M., A. L. Byrd, and E. Barbarese.** 1995. The number of Schmidt-Lanterman incisures is more than doubled in shiverer PNS myelin sheaths. J. Neurocytol. **24:**85–98.
16. **Griffiths, I., M. Klugmann, T. Anderson, D. Yool, C. Thomson, M. H. Schwab, A. Schneider, F. Zimmermann, M. McCulloch, N. Nadon, and K. A. Nave.** 1998. Axonal swellings and degeneration in mice lacking the major proteolipid of myelin. Science **280:**1610–1613.
17. **Grumet, M., A. Flaccus, and R. U. Margolis.** 1993. Functional characterization of chondroitin sulfate proteoglycans of brain: interactions with neurons and neural cell adhesion molecules. J. Cell Biol. **120:**815–824.
18. **Grumet, M., P. Milev, T. Sakurai, L. Karthikeyan, M. Bourdon, R. K. Margolis, and R. U. Margolis.** 1994. Interactions with tenascin and differential effects on cell adhesion of neurocan and phosphacan, two major chondroitin sulfate proteoglycans of nervous tissue. J. Biol. Chem. **269:** 12142–12146.
19. **Haug, F.-M. S.** 1973. Heavy metals in the brain. A light microscopic study in the rat with Timm's sulphide silver method: methodological considerations and cytological and regional staining patterns. Adv. Anat. Embryol. Cell Biol. **47:**1–71.
20. **Haunso, A., M. R. Celio, R. K. Margolis, and P. A. Menoud.** 1999. Phosphacan immunoreactivity is associated with perineuronal nets around parvalbumin-expressing neurones. Brain Res. **834:**219–222.
21. **Holland, S. J., E. Peles, T. Pawson, and J. Schlessinger.** 1998. Cell-contact-dependent signalling in axon growth and guidance: Eph receptor tyrosine kinases and receptor protein tyrosine phosphatase beta. Curr. Opin. Neurobiol. **8:**117–127.
22. **Katoh-Semba, R., and A. Oohira.** 1993. Core proteins of soluble chondroitin sulfate proteoglycans purified from the rat brain block the cell cycle of PC12D cells. J. Cell. Physiol. **156:**17–23.
23. **Kordeli, E., S. Lambert, and V. Bennett.** 1995. AnkyrinG. A new ankyrin gene with neural-specific isoforms localized at the axonal initial segment and node of Ranvier. J. Biol. Chem. **270:**2352–2359.
24. **Krueger, N. X., and H. Saito.** 1992. A human transmembrane protein-tyrosine-phosphatase, PTP zeta, is expressed in brain and has an N-terminal receptor domain homologous to carbonic anhydrases. Proc. Natl. Acad. Sci. USA **89:**7417–7421.
25. **Levy, J. B., P. D. Canoll, O. Silvennoinen, G. Barnea, B. Morse, A. M. Honegger, J. T. Huang, L. A. Cannizzaro, S. H. Park, T. Druck, et al.** 1993. The cloning of a receptor-type protein tyrosine phosphatase expressed in the central nervous system. J. Biol. Chem. **268:**10573–10581.
26. **Li, J., J. W. Tullai, W. H. Yu, and S. R. Salton.** 1998. Regulated expression during development and following sciatic nerve injury of mRNAs encoding the receptor tyrosine phosphatase HPTPzeta/RPTPbeta. Brain Res. Mol. Brain Res. **60:**77–88.
27. **Maeda, N., and M. Noda.** 1996. 6B4 proteoglycan/phosphacan is a repulsive substratum but promotes morphological differentiation of cortical neurons. Development **122:**647–658.
28. **Maeda, N., and M. Noda.** 1998. Involvement of receptor-like protein tyrosine

phosphatase zeta/RPTPbeta and its ligand pleiotrophin/heparin-binding growth-associated molecule (HB-GAM) in neuronal migration. J. Cell Biol. **142:**203–216.
29. **Mansour, S. L., K. R. Thomas, and M. R. Capecchi.** 1988. Disruption of the proto-oncogene int-2 in mouse embryo-derived stem cells: a general strategy for targeting mutations to non-selectable genes. Nature **336:**348–352.
30. **McKeon, R. J., M. J. Jurynec, and C. R. Buck.** 1999. The chondroitin sulfate proteoglycans neurocan and phosphacan are expressed by reactive astrocytes in the chronic CNS glial scar. J. Neurosci. **19:**10778–10788.
31. **Menegoz, M., P. Gaspar, M. Le Bert, T. Galvez, F. Burgaya, C. Palfrey, P. Ezan, F. Arnos, and J. A. Girault.** 1997. Paranodin, a glycoprotein of neuronal paranodal membranes. Neuron **19:**319–331.
32. **Nishizuka, M., S. Ikeda, Y. Arai, N. Maeda, and M. Noda.** 1996. Cell surface-associated extracellular distribution of a neural proteoglycan, 6B4 proteoglycan/phosphacan, in the olfactory epithelium, olfactory nerve, and cells migrating along the olfactory nerve in chick embryos. Neurosci. Res. **24:**345–355.
33. **Ohyama, K., H. Kawano, H. Asou, T. Fukuda, A. Oohira, K. Uyemura, and K. Kawamura.** 1998. Coordinate expression of L1 and 6B4 proteoglycan/phosphacan is correlated with the migration of mesencephalic dopaminergic neurons in mice. Brain Res. Dev. Brain Res. **107:**219–226.
34. **Peles, E., M. Nativ, P. L. Campbell, T. Sakurai, R. Martinez, S. Lev, D. O. Clary, J. Schilling, G. Barnea, G. D. Plowman, et al.** 1995. The carbonic anhydrase domain of receptor tyrosine phosphatase beta is a functional ligand for the axonal cell recognition molecule contactin. Cell **82:**251–260.
35. **Peles, E., M. Nativ, M. Lustig, M. Grumet, J. Schilling, R. Martinez, G. D. Plowman, and J. Schlessinger.** 1997. Identification of a novel contactin-associated transmembrane receptor with multiple domains implicated in protein-protein interactions. EMBO J. **16:**978–988.
36. **Ranjan, M., and L. D. Hudson.** 1996. Regulation of tyrosine phosphorylation and protein tyrosine phosphatases during oligodendrocyte differentiation. Mol. Cell Neurosci. **7:**404–418.
37. **Rasband, M. N., E. Peles, J. S. Trimmer, S. R. Levinson, S. E. Lux, and P. Shrager.** 1999. Dependence of nodal sodium channel clustering on paranodal axoglial contact in the developing CNS. J. Neurosci. **19:**7516–7528.
38. **Rosenbluth, J.** 1966. Redundant myelin sheaths and other ultrastructural features of the toad cerebellum. J. Cell Biol. **28:**73–93.
39. **Rosenbluth, J., W. Stoffel, and R. Schiff.** 1996. Myelin structure in proteolipid protein (PLP)-null mouse spinal cord. J. Comp. Neurol. **371:**336–344.
40. **Sakurai, T., M. Lustig, M. Nativ, J. J. Hemperly, J. Schlessinger, E. Peles, and M. Grumet.** 1997. Induction of neurite outgrowth through contactin and Nr-CAM by extracellular regions of glial receptor tyrosine phosphatase beta. J. Cell Biol. **136:**907–918.
41. **Shintani, T., E. Watanabe, N. Maeda, and M. Noda.** 1998. Neurons as well as astrocytes express proteoglycan-type protein tyrosine phosphatase zeta/RPTPbeta: analysis of mice in which the PTPzeta/RPTPbeta gene was replaced with the LacZ gene. Neurosci. Lett. **247:**135–138.
42. **Soriano, P., C. Montgomery, R. Geske, and A. Bradley.** 1991. Targeted disruption of the c-src proto-oncogene leads to osteopetrosis in mice. Cell **64:**693–702.
43. **Stoker, A., and R. Dutta.** 1998. Protein tyrosine phosphatases and neural development. Bioessays **20:**463–472.